Whispering Gallery Modes-based biosensors for real-time monitoring and binding characterization of antibody-based cancer immunotherapeutics

Freile, Jimena Alvarez; Choukrani, Ghizlane; Zimmermann, Kerstin; Bremer, Edwin; Daehne, Lars

Published in:
Sensors and actuators b-Chemical

DOI:
10.1016/j.snb.2021.130512

Publication date:
2021

Sensors & Actuators: B. Chemical 346 (2021) 130512

Contents lists available at ScienceDirect

Sensors and Actuators: B. Chemical

journal homepage: www.elsevier.com/locate/snb

Whispering Gallery Modes-based biosensors for real-time monitoring and binding characterization of antibody-based cancer immunotherapeutics

Jimena Álvarez Freile [a,b], Ghizlane Choukrani [a,b], Kerstin Zimmermann [a], Edwin Bremer [b,*], Lars Dähne [a]

[a] Surflay Nanotec GmbH, Berlin, Germany
[b] University of Groningen, University Medical Center Groningen, Department of Hematology, Groningen, the Netherlands

ARTICLE INFO

Keywords:
Whispering Gallery Modes
Optical biosensor
Cancer immunotherapy
Drug development
Label-free analytics

ABSTRACT

Development of novel protein-based drugs such as antibodies or immunocytokines and initial validation of target binding typically occurs in 2D settings with e.g., surface plasmon resonance or reflection interferometry using antigen-coated planar sensors. However, a versatile tool to assess binding characteristics of tumour-targeting therapeutics where specific biochemical interactions can be monitored in real-time and in a more realistic 3D interaction setting is currently lacking. Here, we report on the development of versatile small optical 3D biosensors using protein G-coated spherical microparticles based on Whispering Gallery Modes (WGMs). These sensors allowed for an oriented immobilization of theoretically any immunoglobulin G (IgG) and IgG crystallizable fragment domain (Fc)-tagged protein and have been carefully optimized for specific detection of antigen-antibody interactions, as illustrated using the Epithelial Growth Factor Receptor (EGFR) antibody Cetuximab and Program Death Ligand 1 (PD-L1) antibody Atezolizumab. When both ligand and analyte contained an Fc-fragment, protein G binding capacity saturation followed by a "blocking" step with an irrelevant IgG enabled the label-free detection of Fc-tagged antigens with corresponding cognate ligands, as identified using EGFR-Fc, PD-L1-Fc and different members from the tumour necrosis factor receptor family, such as CD27-Fc and 4−1BB-Fc. Thus, WGMs and developed protein G-coated biosensors provide a widely applicable tool to evaluate binding of immunotherapeutics to their targets on the sensor surface, imitating cell surface properties.

1. Introduction

In the last decade, cancer immunotherapeutics including monoclonal antibodies (mAbs) and checkpoint inhibitors, have become key drivers in the biopharmaceutical industry and biomedical research [1]. Their major impact on fighting cancer by boosting the patient's immune system has led to an increasing number of novel formulations [2]. Development of novel protein-based drugs and initial validation of target binding typically occurs in 2D settings, with either surface plasmon resonance (SPR) as the most common analytical platform or reflectance interferometry (RIF) [3]. However, a versatile tool for characterizing the binding profile of tumour-targeting therapeutics where specific multiple molecular interactions can be simultaneously monitored in real-time and in more realistic 3D interaction setting is still lacking. For this purpose, the use of Whispering Gallery Modes (WGM) could provide an excellent means of inexpensive and label-free biomolecule detection [4,5]. The basic principle of WGM-based optical sensors relies on the entrapment of light inside a circular resonator, which acts as an optical cavity. Due to resonance conditions only the so called WGMs are allowed and detected as narrow peaks in the optical spectrum [6–8]. Any modification on the surrounding environment of the resonator (e.g., binding of biomolecules) induces a shift in the WGM wavelength position that is correlated to the total mass of bound molecules. Unlike other sensors (e.g., fluorescent sensors), that usually require analyte labelling or modification, optical resonators detect analytes in their pristine (or native) form. This presents several advantages over label-based counterparts, such as faster analytics, possibility of real-time kinetic studies, and no alteration of bio-affinity due to the incorporated labels [9,10].

WGM-based sensors have been applied in the biomedical field for detection of interleukins or cancer biomarkers [11–13], for determining binding kinetics parameters [14], or monitoring therapy responses [15]. However, more efforts are needed to make WGM-based sensors valuable within the drug development process and biopharmaceutical research.

To date, different WGM resonators have been designed for detecting

* Corresponding author.
E-mail address: E.bremer@umcg.nl (E. Bremer).

https://doi.org/10.1016/j.snb.2021.130512
Received 25 January 2021; Received in revised form 26 July 2021; Accepted 27 July 2021
Available online 30 July 2021

molecular interactions, including glass spheres [13,16] or ring resonators [11,17], with sizes varying from 38 μm to 1 mm. However, in microfluidic devices, as e.g. in the field of organ-on-a-chip, smaller sensors are desired which can work without any connection to the read out instrumentation [18]. Recently, polymer WGM microlaser-based sensors have been integrated into microfluidic chips to perform an ultrasensitive enzyme-linked immunosorbent assay (ELISA) [19], showing the promising potential of micro/nano-photonic technologies to improve current bioanalytical methods. However, the fabrication of such WGM microcavity lasers usually requires advanced technologies to create 3D structures at the micrometre scale [20,21]. Alternatively, a simpler and less time-consuming approach makes use of small fluorescent polystyrene microbead sensors (7−10 μm in diameter), as first shown by P. Mulvaney and M. Himmelhaus [7,22]. These spherical sensors enable monitoring of molecular interactions with high spatial resolution and potentially minimal analyte consumption, as illustrated with the specific binding of streptavidin to biotinylated sensor beads [23,24]. Furthermore, all 2D settings for label-free analytics and most described WGM-based technologies require a solid connection to the transducer (instrumentation). In contrast, the WGM biosensors described here can be located externally from the instrument, such as in microfluidic cells or cell arrays.

During the last decade an easily applicable instrument has been developed [25,26], allowing for interaction studies on the surface of small-sized fluorescent microbeads [24]. Taking advantage of it, here we report WGM-based polystyrene microbeads coated with protein G and validated it for the assessment of label-free detection of several antibody/antigen (Ab-Ag) and cytokine/receptor interactions of great relevance in cancer immunotherapy. Both the spherical shape and the ~10 μm size of our sensors more realistically reflects binding events at the cell surface level. The universal specificity of protein G for binding crystallizable fragment domains (Fc-fragments) of several classes of antibodies (Abs), including all human immunoglobulin G (IgG) subclasses [27], was exploited. As result, immobilization of Abs as well as Fc-based fusion proteins on the sensor surface in different binding approaches, including those where both ligand and analyte were Fc-fragment containing proteins, was achieved. In this way, surface or serum biomarkers for cancer treatment (e.g., Epithelial Growth Factor Receptor (EGFR)) as well as immune checkpoint blockade targets like the Program Death Ligand 1 (PD-L1) and different members of the tumour necrosis factor receptor family, such as 4−1BB and CD27 were immobilized on the sensor surface for the 3-dimensional assessment of binding profile of their corresponding targeted ligand or therapeutic mAb, including the PD-L1 antibody Atezolizumab or EGFR antibody Cetuximab.

2. Materials and methods

2.1. Reagents

Polystyrene based spherical microparticles were produced by Surflay Nanotec GmbH (Berlin, Germany). Poly(sodium-4-styrenesulfonate) (PSS) $MW_{70.000}$, 1-ethyl-3-(3-dimethylaminopropyl) carbodiimide (EDC), salts for buffer solutions, Tween 20, sodium thioglycolate and 2-(N-morpholino) ethanesulfonic acid (MES) were purchased from Sigma-Aldrich (St. Louis, MO). Poly (allylamine hydrochloride) (PAH) $MW_{40.000}$ from Beckmann-Kenko (Bassum, Germany) was further purified by methanol precipitation. N-hydroxysulfosuccinimide (NHS) was obtained from Fluorochem (Hadfield, UK) and 4-(2-hydroxyethyl)-1-piperazineethanesulfonic acid) (HEPES) from Carl Roth GmbH (Karlsruhe, Germany). Bovine serum albumin (BSA) and truncated Streptococcal protein G (G′) with only Fc-binding capabilities were obtained from Sigma-Aldrich. Rhodamine labelled BSA (BSA-Rho) was in house produced by reaction of Rhodamine sulfonylchloride with BSA under basic conditions and dialyses for 5 days. Fc-fusion proteins (EGFR-Fc, CD27-Fc, 4-1BB-Fc, PD-L1-Fc) were purchased from R&D Systems Inc. (Minneapolis, MN). s4-1BBL was taken from Khar Medical (Jerusalem, Israel). hCRP (human C Reactive protein) and anti-hCRP antibody were obtained from P. Miethe (FZMB GmbH, Bad Langensalza, Germany) and Jo-1 (histidyl-transfer ribonucleic acid synthetase) from Diarect AG (Freiburg, Germany). All therapeutic antibodies were obtained from the Hematology department of the University Medical Centre of Groningen (UMCG) (Groningen, The Netherlands).

2.2. Preparation of WGM biosensors

Polystyrene spherical microparticles (Surflay Nanotec GmbH), with refractive index of 1.59, a diameter of 9.44 ± 0.017 μm and containing a coumarin dye (excitation at 395−450 nm and emission band from 450−530 nm), were coated with PAH and PSS by means of Layer-by-Layer (LbL) self-assembly by incubating the particles with aqueous polymer coating solutions [28]. A highly negatively charged polymer containing carboxyl groups was used as final layer of the LbL coating. Particle quantification was done with a Fuchs-Rosenthal counting chamber from Optik Labor (Sussex, UK). Coupling of rhodamine B-labelled bovine serum albumin (BSA-Rho) and unlabelled *Streptococcal* protein G to the carboxyl groups were performed using typical EDC/NHS chemistry [29]. Particles were stored in saline phosphate buffer (PBS) at 4 °C. BSA-Rho coupling was performed to qualitatively assess protein uniformity distribution during coupling and was evaluated by confocal laser scanning microscopy (CLSM) (Leica, TYPE DMI4000 CS, Germany) with an excitation wavelength of 532 nm and an emission wavelength range of 545−625 nm at a photomultiplier voltage of 800 V. Successful coupling of protein G was confirmed by the binding of anti-hCRP by WGM. Changes in signal during the binding of anti-hCRP to protein G modified WGM sensors (protG-WGM sensors) was further used to verify similar quantities of surface coupled protein G for different particle batches. Negative controls were produced to evaluate unspecific binding due to protein adsorption. For this, particles without EDC/NHS treatment but incubated with BSA-Rho were deployed. The specificity of antibody binding to protG-WGM sensor particles was checked with particles modified with a randomly chosen protein (Jo-1) that was coupled following the same procedure as for protein G. Direct coupling of cetuximab (CTX) to the sensor surface was also performed as described above.

2.3. WGM measurements and data evaluation

Measurements were performed on WhisperSense (Fig. S1, *supplementary material*) developed by Surflay and NanoBioAnalytics (Berlin, Germany). A diagram of the experimental setup is shown in Scheme 1A. Sensor particles were added to a six-channel chip from Surflay, based on a well format of Stratec Consumables GmbH (Salzburg, Austria) and a lid of ChipShop (Jena, Germany). Each channel contains 1000 wells of 16 μm diameter and 12 μm depth, so that only one sensor particle fit per well. PBS with 0.05 % Tween20 (PBST) solution was flowed to remove particles not confined to a well, equilibrate the system and get baseline spectra at the beginning of the experiments. Analytes of interest in PBST solution were injected into the fluidic chamber at a flow rate of 40 μL/min using a peristaltic pump (MINIPULS 3 from Gilson, Middleton, WI) and tubing with an inner diameter of 0.50 mm, connected as shown in Scheme 1A. The flowrate did not influence the position of the WGM peaks (data not shown). Online binding was monitored after selecting a single particle and recording its spectra during incubation and rinsing in time intervals of 10 s. For statistical evaluation, single spectra of several particles (at least n = 30) were recorded before and after each binding step. To ensure the same particles are monitored, a long-distance microscope objective and xyz-stage was used to record the exact position of particles in the channel at a nanometer scale (using the “position tool” in the WhisperSense software) at the beginning of each experiment. In this way, the laser beam can interrogate each microparticle one-by-one and mode shifts can be evaluated individually for each microparticle,

avoiding the influence of particle size distribution in the analysis. After every binding step, a washing step with PBST was performed to remove unbound molecules.

All data were analysed by employing a software provided by Nano-BioAnalytics (NBA_Fit_WGM_kinetics) as exemplified in Scheme 1*B*. Spectra collected after each binding step for every single selected particle were stored in separates files, which are finally merged in a single file per particle. A section of the spectra was defined to contain four adjacent peaks with the highest intensity (usually within the wavelength range from 400 to 500 nm) and fitted to obtain the wavelengths (λ) of these four peaks. The position of the first of these four (peak 1) is used to calculate the so called WGM mode shift (Δλ), as the difference between each binding event (λ+ Δλ) and the initial state after equilibration (λ) at the beginning of the experiment. Finally, an average shift is calculated for each binding step as shown in Scheme 1.

2.4. Immobilization of mAbs and Fc-fusion proteins on protG-WGM sensors

Different IgGs, including anti-hCRP and several therapeutic mAbs, such as Cetuximab (CTX) (anti-EGFR), Rituximab (RTX)(anti-CD20) and Atezolizumab (ATZ) (anti-PD-L1) were immobilized on protG-WGM sensors through the binding of their Fc-fragments to protein G [30]. A similar protocol was applied for immobilizing several Fc-tagged proteins (EGFR-Fc, CD27-Fc, 4−1BB-Fc and PD-L1-Fc). For a standard immobilization, 500 µL of protein solution 10 µg/mL in PBST were flowed over protG-WGM sensors for 10 min. To explore the feasibility of our protG-WGM sensors for theoretically all kind of immunoassays, saturation of protein G binding capacity on the sensor surface was explored. For that, online saturation was performed by recirculating 250 µL of protein solution 20 µg/mL for 20 min. Within that time, a shift to longer wavelength in mode position reaching a *plateau* was observed. Alternatively, saturation outside the chip was done by incubating 1 × 10^7protG-WGM sensors with 5 µg of protein in 50 µL of PBS for 30 min under gentle shaking and stored in protein solution until measurement. In both cases, saturation of protein G binding capacity was checked by adding 500 µL 10 µg/mL of a different IgG, (e.g., RTX). If saturation was reached, no further IgG binding should be detected. Once the ligand of interest was immobilized, a solution of analyte at 10 µg/mL was flown through the system for 10 min. After each binding step, analyte solution was removed by rinsing with PBST for 10 min. The amount of total bound molecules per surface area can be calculated according to:

$$\frac{Molecules}{mm^2} = \frac{\sigma \times N_A}{MW} \tag{1}$$

where MW is the protein molecular weight, N_A the Avogadro number and σ represents the adsorbed mass on the surface. The latter is calculated from the radius (R), the known mass density of the adsorbate (ρ), the peak position (λ) and the mode shift (Δλ) as shown in Eqs. (2) and (3) previously discussed in the literature [23].

$$\sigma = \frac{\rho}{3}\,\frac{(R+\Delta R)^3 - R^3}{R^2} \tag{2}$$

$$\Delta R = \frac{R \times \Delta\lambda}{\lambda} \tag{3}$$

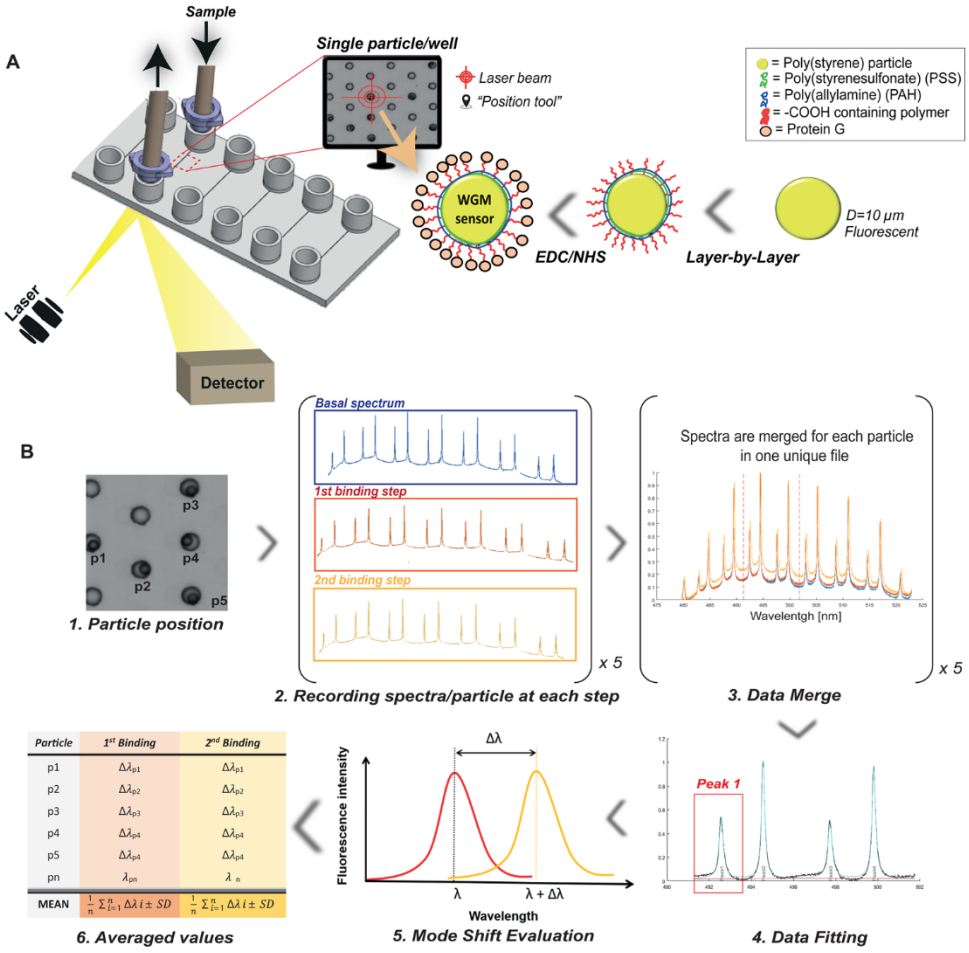

Scheme 1. (A) Experimental setup. A 6-channel microfluidic chip containing 1000 wells/channel of slightly larger dimensions than the sensor beads was used. Wells were filled with the sensors by flushing in an excess of functionalized particles and letting them to sediment. Particles not confined in wells were removed by flushing the channel with water at flow rate of at least 40 µL/min. An online image of the wells was shown on the computer screen. The positions of up to 30 particles were saved by using the "position tool". The laser beam interrogated each particle one-by one and measurements were performed with a spectral resolution of 6 pm. **(B) Data analysis.** Binding of molecules induced a shift in the resonance frequency of the spectrum. Peaks were fitted by software (NBA) and mode shift (Δλ) for an intense mode (Peak 1) was calculated at each binding step for each single particle. Finally, an average shift is calculated for all Δλ values obtained on the 30 selected particles for each binding step.

2.5. Optimizing ligand density and analyte concentration

Sensors with different protein G densities were produced to control ligand density on the sensor surface when protein G binding capacity saturation was required. During coupling, 5×10^6 sensors were incubated with decreasing protein G concentrations ranging from 400 to 6.25 μg/mL in sodium acetate (NaAc) buffer. These particles were used for the immobilization of CTX and further EGFR-Fc binding. For screening purposes or qualitative assays, measuring binding curves for a single analyte concentration is often sufficient. However, to explore the limit of detection of the technology several EGFR-Fc concentrations starting from 37 nM (10 μg/mL) were tested on the best CTX-density found.

2.6. SPR-based studies

SPR ESPRIT Twingle Biosensor platform (KEI, The Netherlands) was used to validate some WGM data. Gold planar chips were firstly pre-functionalized by incubation (o/n) with sodium thioglycolate 1 mM in absolute ethanol at room temperature. Then, protein G was immobilized through EDC/NHS chemistry. IgGs and Fc-fusion proteins were bound to protein G by adding 20 μg/mL of protein in PBS at a flow rate of 16.7 μL/min for 15 min. Saturation of protein G binding capacity was checked by subsequent injections of IgGs and analytes at 10 μg/mL. Data were analysed with KEI kinetic evaluation program. The SPR angle shift in millidegrees (m°) was used as a response unit to quantify the binding of macromolecules to the sensor surface. A change of 122 m ° represents a change in surface protein of approximately 1 ng/mm^2.

2.7. Statistical analysis

Mann-Whitney *U* test [31] was performed to compare sample and control mean values when required. Results with $p < 0.05$ were considered to be significant.

3. Results and discussion

3.1. Oriented immobilization

Protein G has been previously described to considerably increase analyte binding on different biosensors, as it optimally orientates the antigen binding sites to the assay solution [30,32,33]. To test whether this also applied to our system, protein G-oriented versus random immobilization of CTX was compared. Mode shifts for EGFR-Fc binding to CTX were about 12 % higher when CTX was immobilized on protG-WGM sensors ($\Delta\lambda = 93 \pm 3$ pm) compared to random covalent ECD/NHS coupling to the sensor surface ($\Delta\lambda = 83 \pm 5$ pm) (Fig. 1A). Of note, according to literature antigen-binding capacity is 2–8 times higher when oriented immobilization is performed [32]. Therefore, one might have expected a higher difference in the analyte binding signal between random and oriented immobilization of CTX, but it is important to remark that protein G itself has been randomly coupled and some protein G binding sites might be not accessible for the antibody [34]. Importantly, immobilization on protG-WGM sensors does not expose the ligand to any chemical reaction and allows the maintenance of native configuration and binding capacity. In contrast, direct immobilization on the sensor surface typically requires chemical reactions that may impact on bioactivity [35].

3.2. On-line monitoring of Ab-Ag interactions

Protein uniformity on the sensor surface is of great importance to guarantee reproducibility in different series of experiments as millions of sensors are produced within one batch. Coupling of BSA-Rho to the sensor beads showed a homogenous fluorescence intensity between single particles, revealing a uniform protein distribution within and between different sensor batches (Fig. S2). After a qualitative evaluation of protein coupling efficiency, WGM was used for the label-free on-line monitoring of hCRP antibody and hCRP binding on protG-WGM sensors. Specifically, incubation of protG-sensor beads with hCRP antibody yielded a mode-shift of about 150 pm, with subsequent incubation with

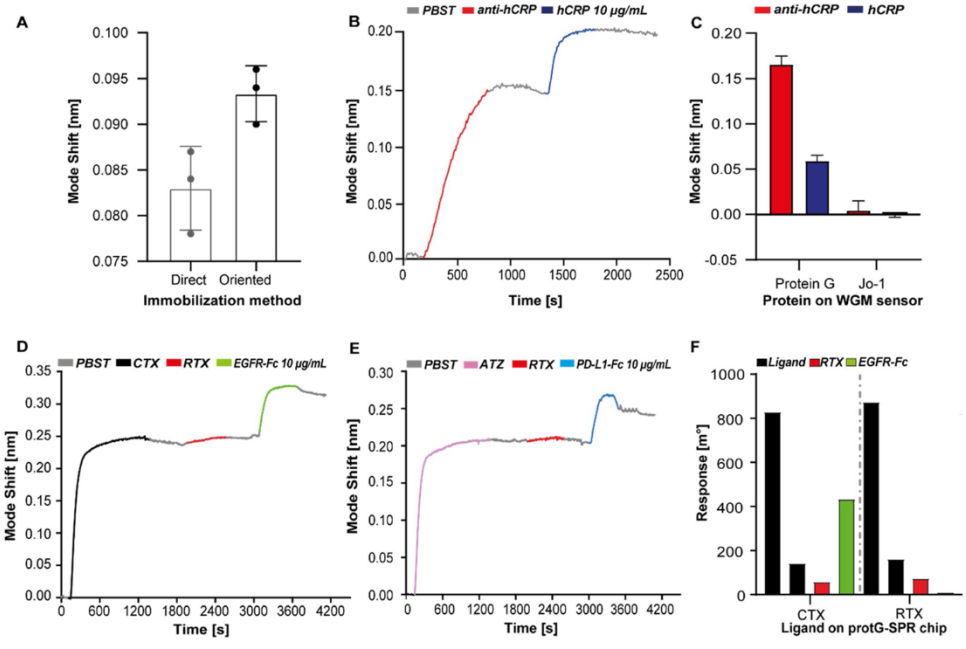

Fig. 1. Oriented immobilization of mAbs on the sensor surface. (A) Mode shift values for EGFR-Fc binding to directly coupled CTX through EDC/NHS chemistry and oriented-immobilized CTX on protG-WGM sensors. Mean ± SD of 3 experiments, 30 beads each (B) Anti-hCRP immobilization on protG-WGM sensors (red) and hCRP binding to the antibody (blue) is shown. Washing steps were performed with PBST (grey); n = 1. (C) Anti-hCRP/hCRP sequential interaction measured on protein G and Jo-1 coated WGM sensors. Mean ± SD of n = 30. (D) On-line monitoring of CTX/EGFR-Fc interaction on protG-WGM sensors. CTX immobilization (black), followed by RTX addition to check binding capacity saturation of protein G (red) and EGFR-Fc binding to CTX (green. (E) On-line monitoring of ATZ/PD-L1-Fc interaction on protG-WGM sensors. ATZ immobilization (pink), followed by RTX addition to check protein G binding capacity saturation (red) and PD-L1 binding to ATZ (blue). (F) Sequential SPR response values for CTX/EGFR-Fc and RTX/EGFR-Fc (control) interactions. Ligand immobilization (black) followed by a second re- binding step to achieve protein G binding capacity saturation, RTX binding control (red) and EGFR-Fc (green) is shown. (For interpretation of the references to colour in this Figure legend, the reader is referred to the web version of this article).

hCRP yielding an additional mode shift of about 60 pm (Fig. 1B). Importantly, no significant mode shifts were detected when WGM sensors coated with control protein histidyl-transfer ribonucleic acid synthetase (Jo-1) were subjected to hCRP antibody or hCRP (Fig. 1C). Taken together, WGM sensors coated with protein G provided a uniform loading capacity and allowed for the on-line label-free analysis of specific Ab-Ag interaction with WGMs. In this way, having many sensor particles differently modified with an antibody of interest and flowing over an analyte (e.g., sample material from one patient, cell culture supernatant, etc) could help to identify the presence of certain molecules in that sample.

3.3. Fc-tagged antigens as analytes

To propose our sensors as a universal bioanalytical tool, feasible for theoretically all kind of immunoassays including those in which antigens are expressed as Fc-fusion constructs (very common tag for recombinant protein purification), saturation of protein G binding capacity on the sensors surface was explored. We found that upon saturating immobilization of the mAbs CTX and ATZ on the sensor surface, addition of a second irrelevant IgG (e.g., RTX) prior to incubation with cognate ligands did not yield a significant additional mode shift (Fig.1D, E), showing that protein-G binding capacity was fully saturated by the mAbs. When binding of recombinant ligands EGFR-Fc and PD-L1-Fc to CTX and ATZ was then evaluated, prominent mode shifts of 91 ± 3 pm and 42 ± 2 pm were obtained respectively (Fig. 1D, E). As result, we showed that by immobilizing mAbs under saturating conditions on protG-WGM sensors, specific Ab-Ag interactions could be detected, even though antigens were expressed as Fc-fusion constructs. SPR-measurements performed similarly as WGM-experiments confirmed that CTX saturation on protein G-modified SPR chips could be also obtained. Thus, a low response of 60 m ° was obtained for RTX binding after CTX saturating binding, whereas a consistent specific response of 436 m ° was obtained for EGFR-Fc binding to CTX (Fig. 1F, S3). Therefore, saturation of protein G-coated sensors by mAbs might be a strategy of interest in other technologies, including SPR. Saturation of protG-WGM sensors outside the microfluidic system might be advantageous if several measurements are planned, as it saves protein and time. We found that incubation of CTX with protG-WGM sensors outside the WGM instrument fully saturated protein G binding capacity, as non-significant mode shifts were observed for further RTX binding (Fig. S4). Further, EGFR-Fc addition yielded a specific mode shift of 90 ± pm (Fig. S4), comparable to those obtained through online saturation.

3.4. Controlling surface ligand density for Fc-tagged analytes

To obtain an optimal window for evaluating ligand/analyte interaction, it is pivotal to define ligand density ranges that yield specific mode shifts. Of note, ligand density in binding assays is usually optimized by testing different ligand concentrations, usually ranging from 2 to 200 μg/mL [36], with simply loading as much ligand as possible to maximize the signal often causing steric hindrance or aggregation problems [37]. Additionally, in the protein G-WGM setting it is important to control the amount of protein G on the sensor surface, as through the quantity of immobilized protein G the amount of surface-bound Fc-fragment containing ligands can be optimized to obtain full saturation and optimal mode-shifts. We found that by decreasing protein G concentration during the coupling procedure, three different protein G densities on the surface could be distinguished: high (protein G concentration >50 μg/mL), medium (25 and 12.5 μg/mL) and low density (<6.25 μg/mL) (Fig. 2A). High-density sensors produced constant mode shift values within the range of 390–420 pm for CTX saturating binding, meaning that either the sensors surface was completely saturated by protein G already at a coupling concentration of 50 μg/mL or even more protein G molecules were coupled on the sensor surface, CTX could not interact with them due to steric hindrance. However, mode shifts for CTX binding on medium and low-density sensors decreased by about 15 % and 60 % respectively compared to high-density ones (Fig. 2A-B). Therefore, ligand density (in this case CTX) could be decreased on the sensor surface, while still reaching protein G binding capacity saturation. Regarding to analyte binding, mode shift values for EGFR-Fc binding to immobilized CTX remained constant (Δλ~90 pm) for high and medium-density sensors but considerably lower (Δλ = 58) on low-density ones (Fig. 2A). This reflects that the ligand loading capacity on low-density sensors was highly decreased and therefore, the analyte signal was diminished as well. When applied to a broader range of Fc-fragment containing ligands, medium-density sensors loaded with CTX, ATZ and PD-L1-Fc produced mode shifts for the binding of their corresponding analytes that were about 4 %, 38 % and 42 % higher than on high-density sensors, respectively (Fig. 2C). Thus, on high-density sensors, steric hindrance is already preventing the binding of the Fc-fragment containing ligands and therefore, negatively affecting the interaction with analyte. Taken together, medium-density sensors gave out an optimal window for evaluating several ligand/analyte interactions when protein G binding capacity saturation required.

3.5. Optimizing analyte concentration

After identifying medium-density sensors as most suited ones, CTX-loaded sensors were evaluated for binding by EGFR-Fc across a dose-range. The lowest EGFR-Fc concentration yielding a detectable signal (Δ15 ± 9 pm) was 0.5 nM (Fig. 2D, S5). An optimal analyte concentration would be the lowest concentration producing a good detectable binding signal. According to our data, EGFR-Fc concentration of 12.3 nM could be considered as optimal as it produced a good value of Δλ = 80 ± 5 pm and with much lower standard deviation than higher concentrations (Fig. 2D). After a nonlinear curve fitting of our data, a dissociation constant (Kd) value of 5.9 ± 3.2 nM was estimated for the CTX/EGFR interaction (Fig. 2E). This value is quite close to the 5 nM obtained through Biacore analysis [38]. These results show that the WGM technology presented here provides not only good qualitative data, but might be also useful for determining kinetic data, as far as the Kd of the interaction is in the nM range (above 5 nM, x10 times higher of the limit of detection). In order to improve the limit of detection and allow for the kinetic studies of interactions with higher affinity (Kd in the low nM or pM range), improvements in the technology microfluidics (e.g., decrease sample dispersion) are still required and will be considered in the near future.

3.6. Imitating cancer cell surface on protG-WGM sensors

ProtG-WGM sensors allow for the immobilization of not only mAbs but also theoretically any Fc-tagged protein. In contrast to planar technologies where ligands are immobilized on planar chips, our setting implies the immobilization of molecules (e.g., cell receptors such as EGFR or PD-L1) on the surface of microspheres, so that the binding events (e.g., binding of target antibodies such as CTX or ATZ) and measurements are carried out in a 3-dimensional miniaturized way. Lymphocytes and cells, where the cell receptors being evaluated are expressed [39–41], are mostly spherical [42] and with a similar size (~10 μm) as our sensors [42,43]. Thus, both the spherical shape and the ~10 μ m size of our sensors more realistically reflects binding events at the cell surface level than planar chips. However, as most of the current therapeutic forms include mAbs (containing Fc-fragments) protein G full binding saturation with the Fc-ligand prior to mAb addition is again required.

Saturating immobilization on protG-WGM sensors of the cell surface biomarker EGFR as well as immune checkpoint blockade targets PD-L1 and costimulatory receptor CD27, all expressed as Fc-fusion proteins, yielded prominent mode shifts (Figs. 3A and 4 A). However, when irrelevant control antibody RTX was added afterwards, mode shifts >100 pm were detected (Figs. 3A and 4 A). Binding of RTX to different

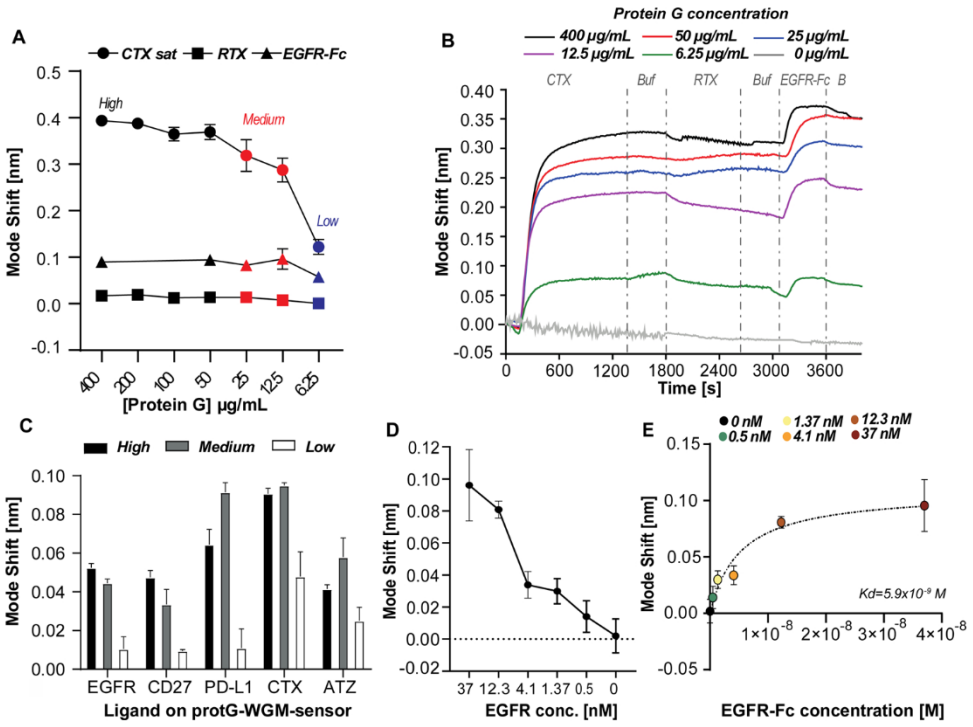

Fig. 2. Optimization of ligand and analyte concentration. (A) Mode shifts for CTX (•), RTX (▮) and EGFR-Fc (▲) binding subsequently flown over sensor particles modified with protein G. Three different protein G densities were established: high (>50 µg/mL), medium (250-125 µg/mL) and low (<6.25 µg/mL). Mean ± SD of n = 30 particles. (B) Binding curves for CTX/EGFR-Fc interaction when different protein G densities were used. Buf = PBST. (C) Analyte binding to cognate ligands immobilized on high, medium, and low-density protG-WGM sensors. Mean and SD of 2 experiments, 30 beads each; Analyte of EGFR is CTX, of CD27 is anti-CD27, of PD-L1 is ATZ, of CTX is EGFR-Fc, and of ATZ is PD-L1-Fc. (D) Dose response curve for the binding of different EGFR-Fc concentrations to CTX-protG-WGM sensors, n = 30 particles. (E) Nonlinear curve fitting for EGFR-Fc binding to CTX according to Michaelis-Menten equation (y = (Ymax*x)/(Kd + x)).

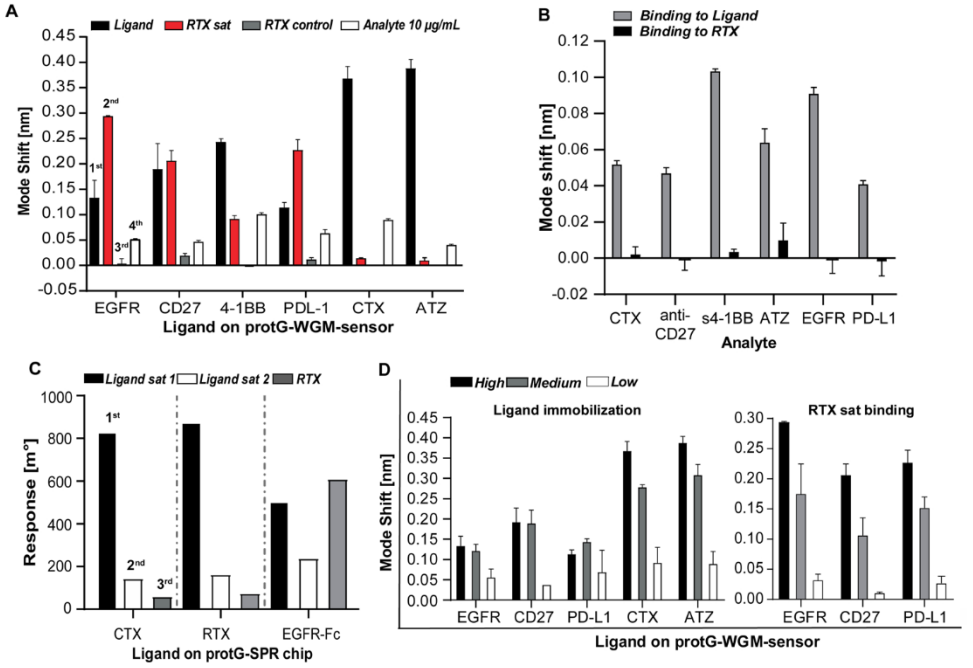

Fig. 3. Immobilization of cell surface cancer biomarkers and immune checkpoint blockade targets for antibody targeting. (A) Sequential averaged mode shift values of different binding studies. Ligand immobilization at saturating conditions (black), followed by RTX addition at high concentration to saturate all free remaining protein G molecules (red) and further RTX addition (dark grey) to check protein G saturation (step not required for IgGs) and analyte addition (light grey) is shown. CTX analyte is EGFR-Fc, anti-CD27 is CD27-Fc, s4-1BB is 4-1BB-Fc, ATZ is PD-L1-Fc, EGFR-Fc is CTX and PD-L1 is ATZ. Mean ± SD of 2 experiments, 30 beads each (B) Mode shift values for the binding of different proteins (analytes) to their immobilized cognate ligand versus bound RTX. Mean ± SD of n = 30 particles (C) Sequential SPR response values for exploring protein G full binding capacity. After two binding steps of CTX and RTX to protein G-coated chips, low further RTX binding was detected, whereas after two binding steps of EGFR-Fc high RTX binding was observed. D) Ligand immobilization and further RTX binding on high, medium, and low-densities protG-WGM sensors. Mean and SD of 2 experiments, each n = 30 particles. (For interpretation of the references to colour in this Figure legend, the reader is referred to the web version of this article).

Fc-tagged proteins was excluded, as mode shifts below the limit of detection were observed (Fig. 3B, S6) when different Fc-const42ructs were flown over RTX immobilized on protG-WGM sensors. These data confirmed that the high mode shifts observed for RTX binding after Fc-fusion protein immobilization must reflect the binding of RTX to the remaining free protein G molecules. To explore whether Fc-fusion proteins are intrinsically unable to achieve saturation of protein G binding capacity or our WGM setting did not facilitate the observation of complete saturation for these Fc containing constructs, several IgGs (RTX, CTX) and Fc-fusion proteins (EGFR-Fc, PDL-1, 4-1BB-Fc, CD-27-Fc) were immobilized on planar SPR chips. When RTX was added after two consecutive IgG/Fc-fusion protein binding steps (to make sure no further binding would occur), small SPR responses (< 100 m °) were obtained after IgGs, whereas a strong increase of 600 m ° was observed after

EGFR-Fc immobilization. Therefore, saturation of protein G binding capacity on SPR chips could only be achieved by IgGs but not Fc-fusion proteins, similarly as on our WGM setting.

In principle, one would expect that Fc-tagged proteins would bind to protG-WGM sensors in a similar way as IgGs, as both contain human IgG1-Fc fragments. However, immobilization of Fc-fusion proteins produced lower mode shifts than IgGs, both in our WGM setting (Fig. 3A) and SPR (Fig. 3C, Fig S7), suggesting that artificially attached domains are able to influence the binding to the sensor surface. The reason for this is not clear. Very few studies have focused on defining differences between Fc-fusion proteins and IgG binding properties to protein G. However, some differences in dynamic binding capacities have been previously observed with various antibodies and Fc-fusion proteins during Protein A chromatography, even those with similar Fc regions. The latter were found to possess higher steric hindrance than antibodies possibly linked to their higher apparent sizes [44]. However, proteins with both lower (e.g., CD27-Fc 126 kDa) and higher (e.g., EGFR-Fc 270 kDa) size than IgGs (~150 kDa) yielded a decreased binding to protein G compared to IgG1 of 51 % and 65 %, respectively (Fig. 3A). Therefore, problems due to steric hindrance might probably originate from 3D folding characteristics rather than size itself. Supporting this hypothesis, we found that by decreasing protein G density on the sensor surface, the maximum amount of loaded IgG (CTX, ATZ) or RTX binding after Fc-fusion protein immobilization decreased, while the amount of Fc-fusion protein remained constant (Fig. 3D). Thus, the maximum number of Fc-fusion protein molecules that could be loaded did not increase even when considerably more protein G molecules were available on the surface. Finally, the binding constant seems not to be affected otherwise flowing over a more potent binding partner (e.g Abs) than a Fc-fusion protein would remove the Fc-fusion protein completely with time and this does not occur (data not shown).

3.7. *On-line monitoring of biotherapeutics binding to cognate Fc-fusion ligands*

The inability of Fc-fusion proteins to saturate protein G binding capacity, forced us to incubate protG-modified particles with RTX after Fc-fusion protein immobilization prior to analyte addition. A second incubation step with RTX did not cause a further increase in mode position, validating that protein G binding capacity was fully saturated then. Importantly, when specific antigen-targeted antibodies were subsequently added, specific mode shifts of 53 ± 2 pm, 65 ± 8 pm and 48 ± 4 pm were detected for EGFR-Fc/CTX, PD-L1-Fc/ATZ and CD27-Fc/anti-CD27 respectively (Figs. 3A and 4 A), proving that the specific binding partner immobilized through its Fc-tag was not removed by RTX.

Blocking of unoccupied binding sites on protein G molecules with RTX or any other irrelevant IgG thus seems pivotal for allowing specific analyte/ligand interaction through this approach. However, it is important to validate that (i) RTX does not interfere with the analyte-ligand interaction and (ii) RTX does not replace already bound ligand molecules on the sensor surface, thereby decreasing sensitivity of the assay. Importantly, mode shift values for s4−1BBL binding (which did not contain an Fc-fragment) to 4−1BB-Fc on the sensor surface were 109 ± 9 pm and 103 ± 3 pm, irrespectively if a pre-incubation step with RTX was performed or not (Fig. 4B, S8). Then, RTX presence on the sensor surface did not alter the interaction between the cytokine receptor 4−1BB-Fc and its recombinant ligand s4−1BBL. Further, the percentage of total bound molecules (Fc-fusion protein sat + RTX sat) per surface area was calculated considering the amount of total bound CTX to protein G as the maximal loading capacity (100 %). Values of 100 and 110 % were obtained for [CD27-Fc + RTX] and [PD-L1-Fc + RTX], respectively (Fig. S9). If already surface bound Fc-tagged proteins would have been completely replaced by RTX, values close to 100 % would be expected together with a total undetectable analyte binding. However, considerable anti-CD27 or ATZ binding signals were still observed (Fig. 4A), meaning that RTX merely functions as a placeholder to occupy any remaining protein G molecules. For [EGFR-Fc + RTX] and [4−1BB-Fc + RTX], the estimated percentage of total bound molecules was lower (Fig. S9). As previously discussed, theoretically more molecules could bind to the sensors, but they do not presumably because steric hindrance impedes their access to free protein G molecules. When this "blocking" strategy was tested on SPR, a specific SPR response for PD-L1-Fc binding to immobilized ATZ was detected (Fig. 4C, Fig S10). Instead of RTX, theoretically any other irrelevant IgG could be used as "blocking" agent for protein G, and even Fc fragments themselves, which might be a better alternative due to their smaller size (~50 kDa). However, according to our data full saturation of protein G binding capacity could be achieved with IgGs but not by other Fc-fusion protein. Thus, when CD27-Fc was added after immobilizing EGFR-Fc on the sensor surface and vice versa, they could not prevent further RTX binding (Fig. 4D). Further, in the latter scenery not even EGFR-Fc binding was observed, most probably due to steric hindrance effects as EGFR is much bigger than CD27. Again, it seems that IgGs because of their spatial conformation and three-dimensional structure resembling the capital letter Y

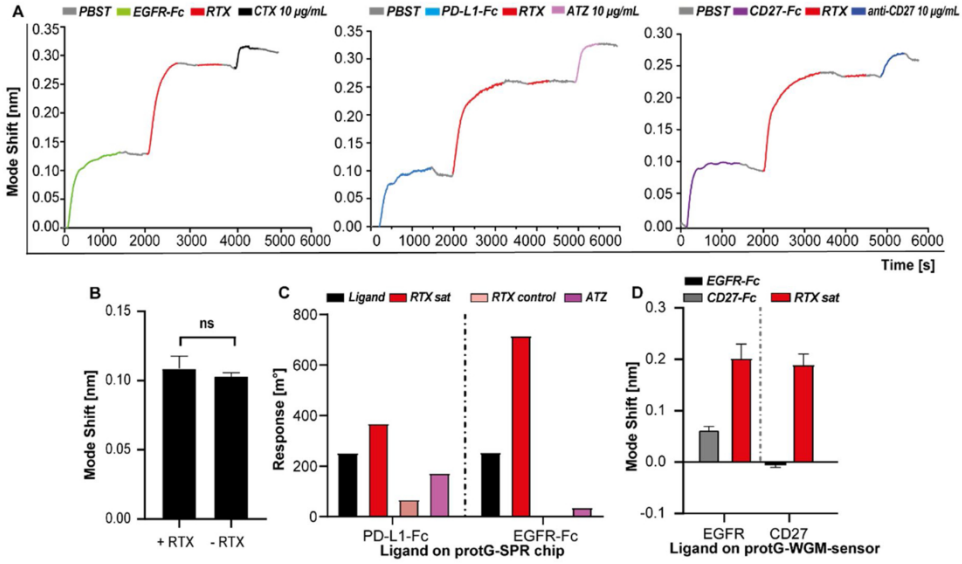

Fig. 4. RTX blocking strategy to overcome Fc-fusion proteins inability for protein G binding capacity saturation on protG-WGM sensors and SPR gold chips. A) On-line monitoring of EGFR-Fc/CTX (left), PD-L1-Fc/ATZ (middle) and CD27-Fc/anti-CD27 (right) interactions on protG-WGM sensors. Ligand immobilization followed by two RTX binding steps and analyte binding is shown. A first RTX binding step saturates protein G binding capacity and a second proves for complete saturation before analyte is added. (B) Averaged mode shift values for s-41BBL binding to 4-1BB-Fc with and without RTX on the sensor surface. Mean ± SD of n = 3 experiments, 30 particles each. (C) Sequential SPR response values for PD-L1-Fc/ATZ interaction, including a RTX "blocking" step prior to ATZ addition. EGFR-Fc was used instead of PD-L1-Fc as negative control. (D) Blocking of free remaining protein G binding capacity by non-targeted Fc-fusion proteins. CD27-Fc was added after saturating immobilization of EGFR-Fc (left) and vice versa (right). Mean ± SD of n = 30 particles.

can easily access available free protein G molecules.

4. Conclusion

In this article, we report on the development of new versatile universal optical biosensors using protein G-coated spherical microparticles as WGMs resonators. We have used fluorescent spherical microbeads with diameter of about 10 μm as optical resonators to study the interactions between therapeutic monoclonal antibodies (mAbs) and proteins expressed by cancer cells. These WGM-based sensors allow for an oriented immobilization of theoretically any IgG and Fc-tagged protein and have been carefully optimized for detecting specific interactions and minimizing unspecific binding. Both mAbs and Fc-fusion proteins were oriented on the sensor surface by utilizing the high affinity binding between Fc-domains and protein G. Several experimental settings have been investigated, including those in which both antigen and analyte were Fc-fragment containing molecules. In that case, protein G binding capacity saturation was explored. We found differences in binding properties between IgGs and Fc-fusion proteins. While protein G binding capacity saturation could be easily achieved by native IgGs, saturation by Fc-fusion proteins could not be observed. Therefore, a pre-incubation step of the fusion protein-loaded sensors with a non-targeted antibody was necessary in order to prevent analyte binding via the Fc-domain. In this way and as proof-of-concept, cell surface biomarkers as well as immune checkpoint blockade targets were immobilized on sensors, to imitate the proteinaceous exterior of cell surfaces, for monitoring label-free binding of therapeutic mAbs and their corresponding ligands present on (tumour) cells. This study demonstrates that the small WGMs optical biosensors presented here provide a versatile 3-dimensional assessment of binding characteristics that consume tiny amounts of analyte per sensor and allows a high statistical safety, which is hardly possible by other label-free methods like SPR or RIF. Hence, this technology is very useful for routine assessment of novel cancer therapeutic formulations or the detection of serum components of patient samples, including specific biomarkers

CRediT authorship contribution statement

Jimena Álvarez Freile: Sensor preparation, WGM measurements, SPR studies, data analysis and writing of the manuscript. **Ghizlane Choukrani:** Sensor preparation, characterization. **Kerstin Zimmermann:** Protein interaction specialist, kinetics, experimental design, data analysis and reviewing, of the manuscript. **Edwin Bremer:** Cancer research, supervisor medical direction, experimental design, data analysis, writing and editing of the manuscript. **Lars Dähne:** Supervisor chemical direction, Whispering Gallery Mode technology, reviewing, editing of the manuscript.

Declaration of Competing Interest

The authors declare that they have no known competing financial interests or personal relationships that could have appeared to influence the work reported in this paper.

Acknowledgements

The authors thank various members of Surflay Nanotec GmbH, especially Mateusz Olszyna for his review of the manuscript, Christian Funk for the preparation of polystyrene particles, Dr. Gabriella Egri for the fluorescent-labelled material, Dr. Wei Wan and Dr. Aline Debrassi for their constructive feedback. Additionally, we thank Kristina Mykhailiuk from Scienion AG (Berlin, Germany) for helping us to perform SPR studies. The work was supported by the European Commission under GA number813871 - i-DireCT.

Appendix A. Supplementary data

Supplementary material related to this article can be found, in the online version, at doi:https://doi.org/10.1016/j.snb.2021.130512.

References

[1] L. Urquhart, Market watch: top drugs and companies by sales in 2017, Nat. Rev. Drug Discov. 17 (2018) 232, https://doi.org/10.1038/nrd.2018.42.
[2] V. Sifniotis, E. Cruz, B. Eroglu, V. Kayser, Current advancements in addressing key challenges of therapeutic antibody design, manufacture, and formulation, Antibodies 8 (2019) 36, https://doi.org/10.3390/antib8020036.
[3] M. Gavutis, S. Lata, P. Lamken, P. Müller, J. Piehler, Lateral ligand-receptor interactions on membranes probed by simultaneous fluorescence-interference detection, Biophys. J. 88 (2005) 4289–4302, https://doi.org/10.1529/biophysj.104.055855.
[4] W. Pongruengkiat, S. Pechprasarn, Whispering-gallery mode resonators for detecting cancer, Sensors (Switzerland) 17 (2017), https://doi.org/10.3390/s17092095.
[5] E. Kim, M.D. Baaske, F. Vollmer, Towards next-generation label-free biosensors: recent advances in whispering gallery mode sensors, Lab Chip 17 (2017) 1190–1205, https://doi.org/10.1039/c6lc01595f.
[6] F. Vollmer, S. Arnold, Whispering-gallery-mode biosensing: label-free detection down to single molecules, Nat. Methods 5 (2008) 591–596, https://doi.org/10.1038/nmeth.1221.
[7] A. Francois, M. Himmelhaus, Optical sensors based on whispering gallery modes in fluorescent microbeads: size dependence and influence of substrate, Sensors 9 (2009) 6836–6852, https://doi.org/10.3390/s90906836.
[8] R. Bischler, M. Olszyna, M. Himmelhaus, L. Dähne, Development of a fully automated in-vitro diagnostics system based on low-Q whispering gallery modes in fluorescent microparticles, Eur. Phys. J. Spec. Top. 223 (2014) 2041–2055, https://doi.org/10.1140/epjst/e2014-02247-2.
[9] M.K. Quinn, N. Gnan, S. James, A. Ninarello, F. Sciortino, E. Zaccarelli, J. J. McManus, How fluorescent labelling alters the solution behaviour of proteins, Phys. Chem. Chem. Phys. 17 (2015) 31177–31187, https://doi.org/10.1039/c5cp04463d.
[10] T. Rinken, State of the Art in Biosensors - General Aspects, InTech, 2013, https://doi.org/10.5772/45832.
[11] J.T. Gohring, P.S. Dale, X. Fan, Detection of HER2 breast cancer biomarker using the opto-fluidic ring resonator biosensor, Sensors Actuators, B Chem. 146 (2010) 226–230, https://doi.org/10.1016/j.snb.2010.01.067.
[12] H. Zhu, P.S. Dale, C.W. Caldwell, X. Fan, Rapid and label-free detection of breast cancer biomarker CA15-3 in clinical human serum samples with optofluidic ring resonator sensors, Anal. Chem. 81 (2009) 9858–9865, https://doi.org/10.1021/ac902437g.
[13] H.A. Huckabay, R.C. Dunn, Whispering gallery mode imaging for the multiplexed detection of biomarkers, Sensors Actuators, B Chem. 160 (2011) 1262–1267, https://doi.org/10.1016/j.snb.2011.09.060.
[14] C.E. Soteropulos, H.K. Hunt, A.M. Armani, Determination of binding kinetics using whispering gallery mode microcavities, Appl. Phys. Lett. 99 (2011), https://doi.org/10.1063/1.3634023.
[15] Y.J. Chen, U. Schoeler, C.H.B. Huang, F. Vollmer, Combining whispering-gallery mode optical biosensors with microfluidics for real-time detection of protein secretion from living cells in complex media, Small 14 (2018), https://doi.org/10.1002/smll.201703705.
[16] H. Wang, L. Yuan, C.W. Kim, X. Lan, J. Huang, Y. Ma, H. Xiao, Integrated chemical vapor sensor based on thin wall capillary coupled porous glass microsphere optical resonator, Sensors Actuators, B Chem. 216 (2015) 332–336, https://doi.org/10.1016/j.snb.2015.04.012.
[17] J.D. Suter, D.J. Howard, H. Shi, C.W. Caldwell, X. Fan, Label-free DNA methylation analysis using opto-fluidic ring resonators, Biosens. Bioelectron. 26 (2010) 1016–1020, https://doi.org/10.1016/j.bios.2010.08.050.
[18] E. Dervisevic, K.L. Tuck, N.H. Voelcker, V.J. Cadarso, Recent progress in lab-on-a-chip systems for the monitoring of metabolites for mammalian and microbial cell research, Sensors 19 (2019).
[19] X. Ouyang, T. Liu, Y. Zhang, J. He, Z. He, A.P. Zhang, H.Y. Tam, Ultrasensitive optofluidic enzyme-linked immunosorbent assay by on-chip integrated polymer whispering-gallery-mode microlaser sensors, Lab Chip 20 (2020) 2438–2446, https://doi.org/10.1039/d0lc00240b.
[20] K. De Vos, I. Bartolozzi, E. Schacht, P. Bienstman, R. Baets, Silicon-on-Insulator microring resonator for sensitive and label-free biosensing, Opt. Express 15 (2007) 7610, https://doi.org/10.1364/oe.15.007610.
[21] S.F. Wondimu, M. Hippler, C. Hussal, A. Hofmann, S. Krämmer, J. Lahann, H. Kalt, W. Freude, C. Koos, Robust label-free biosensing using microdisk laser arrays with on-chip references, Opt. Express 26 (2018) 3161, https://doi.org/10.1364/oe.26.003161.
[22] E. Nuhiji, P. Mulvaney, Detection of unlabeled oligonucleotide targets using whispering gallery modes in single, fluorescent microspheres, Small 3 (2007) 1408–1414, https://doi.org/10.1002/smll.200600676.
[23] M. Himmelhaus, S. Krishnamoorthy, A. Francois, Optical sensors based on whispering gallery modes in fluorescent microbeads: response to specific interactions, Sensors 10 (2010) 6257–6274, https://doi.org/10.3390/s100606257.
[24] M. Olszyna, A. Debrassi, C. Üzüm, L. Dähne, Label-free bioanalysis based on Low-Q whispering gallery modes: rapid preparation of microsensors by means of layer-by-

Layer technology, Adv. Funct. Mater. 29 (2018) 1–7, https://doi.org/10.1002/adfm.201805998.
[25] WhisperSense & NanoCoater | Surflay Nanotec, (n.d.). https://www.surflay.com/en/products/devices (accessed April 27, 2021).
[26] WhisperSense: Microsensors for Bioanalysis, (n.d.). http://www.whisense.com/ (accessed April 27, 2021).
[27] L. Björck, G. Kronvall, Purification and some properties of streptococcal protein G, a novel IgG-binding reagent, J. Immunol. 133 (1984).
[28] C.S. Peyratout, L. Dähne, Tailor-made polyelectrolyte microcapsules: from multilayers to smart containers, Angew. Chemie - Int. Ed. 43 (2004) 3762–3783, https://doi.org/10.1002/anie.200300568.
[29] G.T. Hermanson, Bioconjugate Techniques, 2013 (accessed January 10, 2021), https://books.google.de/books?hl=es&lr=&id=6aO-207lhdgC&oi=fnd&pg=PP1&ots=aL-Gv6HoVT&sig=m3Wn1iQuJJaNbio7h0-JSvJnNng&redir_esc=y#v=onepage&q&f=false.
[30] S.K. Vashist, C.K. Dixit, B.D. MacCraith, R. O'Kennedy, Effect of antibody immobilization strategies on the analytical performance of a surface plasmon resonance-based immunoassay, Analyst 136 (2011) 4431–4436, https://doi.org/10.1039/c1an15325k.
[31] N. Nachar, The Mann-Whitney U: a test for assessing whether two independent samples come from the same distribution, Tutor. Quant. Methods Psychol. 4 (2008) 13–20, https://doi.org/10.20982/tqmp.04.1.p013.
[32] A. Kausaite-Minkstimiene, A. Ramanaviciene, J. Kirlyte, A. Ramanavicius, Comparative study of random and oriented antibody immobilization techniques on the binding capacity of immunosensor, Anal. Chem. 82 (2010) 6401–6408, https://doi.org/10.1021/ac100468k.
[33] J.S. Seo, S. Lee, C.D. Poulter, Regioselective covalent immobilization of recombinant antibody-binding proteins A, G, and L for construction of antibody arrays, J. Am. Chem. Soc. 135 (2013) 8973–8980, https://doi.org/10.1021/ja402447g.
[34] M. Shen, J.F. Rusling, C.K. Dixit, Site-selective orientated immobilization of antibodies and conjugates for immunodiagnostics development, Methods 116 (2017) 95–111, https://doi.org/10.1016/j.ymeth.2016.11.010.
[35] E. Helmerhorst, D.J. Chandler, M. Nussio, C.D. Mamotte, Real-time and label-free bio-sensing of molecular interactions by surface plasmon resonance: a laboratory medicine perspective, Clin. Biochem. Rev. 33 (2012) 161–173.
[36] D.G. Drescher, M.J. Drescher, N.A. Ramakrishnan, Surface plasmon resonance (SPR) analysis of binding interactions of proteins in inner-ear sensory epithelia, Methods Mol. Biol. 493 (2009) 323–343, https://doi.org/10.1007/978-1-59745-523-7_20.
[37] H. Zhao, L.F. Boyd, P. Schuck, Measuring protein interactions by optical biosensors, Curr. Protoc. Protein Sci. 2017 (2017) 1–25, https://doi.org/10.1002/cpps.31.
[38] D. Patel, A. Lahiji, S. Patel, M. Franklin, X. Jimenez, D.J. Hicklin, X. Kang, Monoclonal antibody cetuximab binds to and down-regulates constitutively activated epidermal growth factor receptor vIII on the cell surface, Anticancer Res. 27 (2007) 3355–3366.
[39] A. Rotte, J.Y. Jin, V. Lemaire, Mechanistic overview of immune checkpoints to support the rational design of their combinations in cancer immunotherapy, Ann. Oncol. 29 (2018) 71–83, https://doi.org/10.1093/annonc/mdx686.
[40] H. Guan, Y. Wan, J. Lan, Q. Wang, Z. Wang, Y. Li, J. Zheng, X. Zhang, Z. Wang, Y. Shen, F. Xie, PD-L1 is a critical mediator of regulatory B cells and T cells in invasive breast cancer, Sci. Rep. 6 (2016) 1–10, https://doi.org/10.1038/srep35651.
[41] A.M. Starzer, A.S. Berghoff, New emerging targets in cancer immunotherapy: CD27 (TNFRSF7), ESMO Open 4 (2020), https://doi.org/10.1136/esmoopen-2019-000629.
[42] M.J. Brown, J.A. Hallam, E. Colucci-Guyon, S. Shaw, Rigidity of circulating lymphocytes is primarily conferred by vimentin intermediate filaments, J. Immunol. 166 (2001) 6640–6646, https://doi.org/10.4049/jimmunol.166.11.6640.
[43] R.L.E. Cano, H.D.E. Lopera, Introduction to T and B Lymphocytes, 2013 (accessed July 15, 2020), https://www.ncbi.nlm.nih.gov/books/NBK459471/.
[44] S. Ghose, B. Hubbard, S.M. Cramer, Binding capacity differences for antibodies and Fc-fusion proteins on protein A chromatographic materials, Biotechnol. Bioeng. 96 (2007) 768–779, https://doi.org/10.1002/bit.21044.

Jimena Álvarez Freile PhD candidate at the Hematology Dept., University of Groningen, The Netherlands and ESR3 at i-DireCT project (Horizon 2020). Received her B.S. degree in Biotechnology from the University of Oviedo, Spain in 2018 and her M.S. in Oncology and Cancer Biology from the University of Salamanca, Spain in 2019. Her fields of interest include biosensing devices and nanotech-based drug formulations.

Ghizlane Choukrani PhD candidate at the Hematology Dept., University of Groningen, Groningen, The Netherlands and ESR4 at i-DireCT project (Horizon 2020). Received her M.S in Bio-nanosystem Engineering from Chonbuk National University, South Korea in 2019. Her field of interests include nanotechnology, material science and nano-drug delivery systems.

Kerstin Zimmermann Received her Ph.D degree from the Humboldt University, Berlin in 2008. In 2010she started a post-doctoral position at UMass Medical School, University of Massachusetts, where she stayed for 7 years. Since April 2017 she works as Project Manager and Scientist at Surflay Nanotec GmbH. Her fields of interest and expertise are protein-protein interactions, Surface Plasmon Resonance, bioanalytical platforms, and modification of sensor surfaces.

Prof. Dr. Edwin Bremer is a tenure track Professor at the UMCG where he is chair of the section Immunohematology. He was an honorary Associate Professor at Exeter University Medical School (2014–2017) and is Visiting Professor in Harbin (China, 2011-current) and Edmonton (Canada, 2013). His research interests include tumor immunology and immunotherapy, in particular antibody-engineering and antibody-based immunocytokines. He has >45 peer-reviewed articles in the field.

Dr. habil. Lars Dähne is the founder and CEO Surflay Nanotec GmbH since 2008. He started research on nanocoatings and Layer-by-Layer technology in 1998 at the Max-Planck-Institute of Colloids and Interfaces. In 2001 he co-founded the biotech company Capsulution NanoScience AG, he contributed to the discovery of LbL coated colloidal systems and their applications. During his career he has published numerous patents and more than 70 peer-reviewed articles. His field of interest and expertise include Layer-by-Layer technology, microsensors and polymers.